Journal of Applied Polymer Science

Poly(lactic acid)/Halloysite Nanotubes Nanocomposites: Structure, Thermal, and Mechanical Properties as a Function of Halloysite Treatment

Kalappa Prashantha,[1,2] Benoît Lecouvet,[3] Michel Sclavons,[3] Marie France Lacrampe,[1,2] Patricia Krawczak[1,2]

[1]Ecole des Mines de Douai, Department of Polymers and Composites Technology and Mechanical Engineering, 941 rue Charles Bourseul, CS 10838, F-59508 Douai Cedex France

[2]Université Lille Nord de France, F-59000, Lille, France

[3]Institute of Condensed Matter and Nanosciences (IMCN), Université Catholique de Louvain, Place Pasteur 1, B-1348 Louvain-la-Neuve, Belgium

Correspondence to: M. F. Lacrampe (E-mail: marie-france.lacrampe@mines-douai.fr)

ABSTRACT: Poly(lactic acid) (PLA)/halloysite nanotubes (HNT) nanocomposites were prepared by melt extrusion using a masterbatch dilution process. Effect of addition of both unmodified halloysites (HNT) and quaternary ammonium salt treated halloysites (m-HNT) was investigated at different nanofiller contents. A homogeneous distribution/dispersion of halloysites in the PLA matrix is obtained for both unmodified and modified nanotubes within the studied composition range. The nucleating effect of halloysites, resulting in a limited increase of degree of crystallinity, is more pronounced in the case of m-HNT. Besides, the rigidity, tensile, flexural, and impact resistances of PLA significantly increase on addition of halloysites, the property improvement being higher for m-HNT than for HNT. Interestingly, there is no significant embrittlement (almost constant elongation at break). Based on micromechanical models, this superior reinforcement efficiency of m-HNT was ascribed to the better interfacial compatibility induced by the modification of the nanotube surface. © 2012 Wiley Periodicals, Inc. J. Appl. Polym. Sci. 000: 000–000, 2012

KEYWORDS: biopolymers and renewable polymers; composites; mechanical properties; structure–property relations

Received 8 June 2012; accepted 18 July 2012; published online
DOI: 10.1002/app.38358

INTRODUCTION

It is rather widely admitted that biodegradable, compostable and/or bio-based polymers could have a well-grounded role in reducing environmental issues for the plastic industry.[1,2] In the family of bio-based polymers, poly(lactic acid) (PLA) appears to be one of the most attractive material for applications in agriculture, biomedical devices, and as a packaging material,[3] because of its availability, compostability, and biocompatibility properties. However, its use for a large variety of industrial applications still requires tuning or adapting its mechanical properties.

Recently, many studies were reported aiming at improving the thermomechanical and barrier properties of pristine PLA by incorporating a small amount of nanofiller such as clays[4–7] and carbon nanotubes (CNTs)[8,9] to produce compostable polymeric nanocomposite materials with improved thermomechanical performance. However, addition of CNTs into polymers increases strength at the expense of ductility.[10] In addition, CNTs relatively high cost, large scale production, safety, and health issues still need to be addressed before wider industrial implementation. Similarly, achieving fully exfoliated structure of layered silicates such as montmorillonites (MMTs) in polymer matrices is rather difficult.[11] Halloysite nanotubes (HNTs) have recently become the subject of research interest as a new type of nanofiller for enhancing the mechanical, thermal, and fire-retardant performance of polymers.[7,12–17] Their melt blending and their reinforcement potential in the case of PLA matrices still need to be investigated.

HNTs are natural aluminosilicate nanotubes from a clay mineral with a similar structure to kaolinite. They have 1 : 1 layered aluminosilicate structure, in which the hollow tubular morphology is formed by layer rolling. HNTs exhibit a high aspect ratio with nanotube length of 1–15 μm with inner and outer diameters of 15–100 nm and 40–120 nm, respectively.[18] Compared to CNTs, HNTs are easily available, abundant, biocompatible, and much

cheaper. The rodlike geometry of HNTs never intertwines each other, which makes HNTs disperse in a polymer matrix better than CNTs. This is due to their unique crystal structure, low density of hydroxyl functional groups, and their tubular shape.[19,20] In addition, only traces of heavy metals were detected, much lower than European Union standards on the restriction of harmful substances.[18] Entrusting aforementioned features, HNTs have been incorporated into various polymers including biopolymers,[21,22] but rarely reported on PLA.[7] Previous studies from our laboratory[15–17] and in the literature[12–14] indicate that incorporation of HNTs improves the thermomechanical properties of the nanocomposites. Unlike, other nanofillers such as CNTs and MMT, HNTs provides strength increase without loss of ductility. Importantly, HNTs are biocompatible materials and their usage in drug delivery, bioreactors, and genes delivery applications is well established in the literature.[23–27] Thus, polymer nanocomposites with functional criteria, including biocompatibility, compostability, and mechanical properties may be designed by using HNTs as filler in PLA matrix.

In this context, this article aims at developing such PLA/HNTs nanocomposites by melt compounding via a masterbatch dilution process. Effect of HNTs treatment on the morphology, crystallization behavior, dynamic mechanical, and usage (i.e., tensile, bending, and impact) properties of nanocomposites was investigated.

EXPERIMENTAL

Materials

The compounds developed in this study were prepared from PLA (4032D, Nature Works®) and both unmodified HNTs and quaternary ammonium salt with benzoalkonium chloride treated HNTs nanotubes (m-HNT) of 2% functionality with a decomposition temperature of 225°C (Natural Nano) having an average diameter of 80 nm, a length of about 1.2 microns, and a density of 2.5 g/cm^3. All the materials were dried under vacuum at 80°C for 4 h before processing

Preparation of Masterbatch

Masterbatch dilution technique was adopted to prepare nanocomposites of the desired halloysite content. Therefore, masterbatches containing 15 wt % of halloysites were prepared by melt blending HNT or m-HNT in PLA matrix using a twin-screw extruder (Haake Polylab OS, Thermoscientific) equipped with a screw of $D = 16$ mm diameter and L/D = 40 length to diameter ratio. The temperature profile in the extruder was set at 160°C in the feed zone, sequentially at 170, 173, 175, and 177°C in the metering zone, and 180°C at the die. This processing temperature window falls well below the decomposition temperature (225°C) of the quaternary ammonium salt with benzoalkonium chloride modifier of the halloysites.[28] The screw speed and feed rate were set at 40 rpm and 1000 g h^{-1}, respectively. Extruded material was cut into small pellets in a pelletizer (SGS 25-E4, Scheer, Germany). Masterbatch pellets were dried at 80°C in vacuum oven for overnight to remove residual water content for further utilization.

Processing of Nanocomposites

PLA/HNT and PLA/m-HNT nanocomposites were produced by melt compounding by mixing neat PLA granules with the masterbatch pellets containing 15 wt % of halloysites. The dilution was carried out in a single-screw extruder (Rheocord System 40, Haake Buchler Product, Germany) at a screw speed of 50 rpm. The temperatures setting from the hopper to the die was 165/170/175/180°C. A mass of 2 kg was extruded for each composition using similar processing conditions. During melt extrusion, ventilation was kept on to remove trapped air in the compounds. Nanocomposites bearing 2, 4, and 6 wt % fillers in the PLA matrix were fabricated. Unfilled PLA pellets were processed under the same conditions to get a reference material (same thermal history). After pelletizing, the nanocomposite and PLA granules were dried for 5 h under vacuum at 80°C before injection moulding.

Standard test specimens for tensile, impact, flexural, and dynamic mechanical analysis (DMA) were molded using an electric injection molding machine (KM80-160E, KraussMaffei, Germany). The temperature profile setting ranged from 160 to 195°C and the mold temperature was maintained at 35°C due to water cooling. The holding pressure and screw rotation speed were 350 bar and 100 rpm, respectively with a throughput of 50 cm^3 s^{-1}.

Morphological Characterization

Samples for scanning electron microscopy (SEM) were prepared by coating a thin layer of carbon onto the cryofractured nanocomposite samples. SEM imaging of the nanocomposites was performed under high vacuum with a SEM instrument (S-4300SE/N, Hitachi, Japan) operating at 5 kV.

Specimens for transmission electron microscopy (TEM) analysis were cut from bulk samples using a microtome (Reichert, Switzerland). Ultrathin sections of approximately 95 nm in thickness were cut using an ultra-diamond knife with a cut angle of 35° (Diatome, Switzerland) and collected on 400 mesh copper grids. TEM images were obtained using a TEM instrument (LEO 922, Zeiss, Germany) with a 200 kV acceleration voltage.

Thermal Analysis

Melting and crystallization behavior was studied in nonisothermal conditions under nitrogen atmosphere by differential scanning calorimetry (DSC 7 Perkin-Elmer). The sample was heated from 30 to 200°C at 10°C min^{-1}, held at 200°C to eliminate any previous thermal history, and then cooled to 30°C at 10°C min^{-1}. The samples were kept at this temperature for another 5 min and heated again to 200°C at 10°C min^{-1}. The glass transition temperature (T_g), crystallization temperature (T_c), melting temperature (T_m), crystallization enthalpy (ΔH_c), and melting enthalpy (ΔH_m) were determined. The crystal weight fraction (X_c) of PLA and its nanocomposites was calculated using eq. (1):

$$X_c = \frac{\Delta H_m - H_c}{\Delta H_m^0 (1 - w_t)} \quad (1)$$

where ΔH_c is the crystallization enthalpy, ΔH_m^0 is the melting enthalpy for 100% crystalline sample ($\Delta H_c = 93.7$ J g^{-1}),[29] W_t is the filler weight fraction in the nanocomposites.

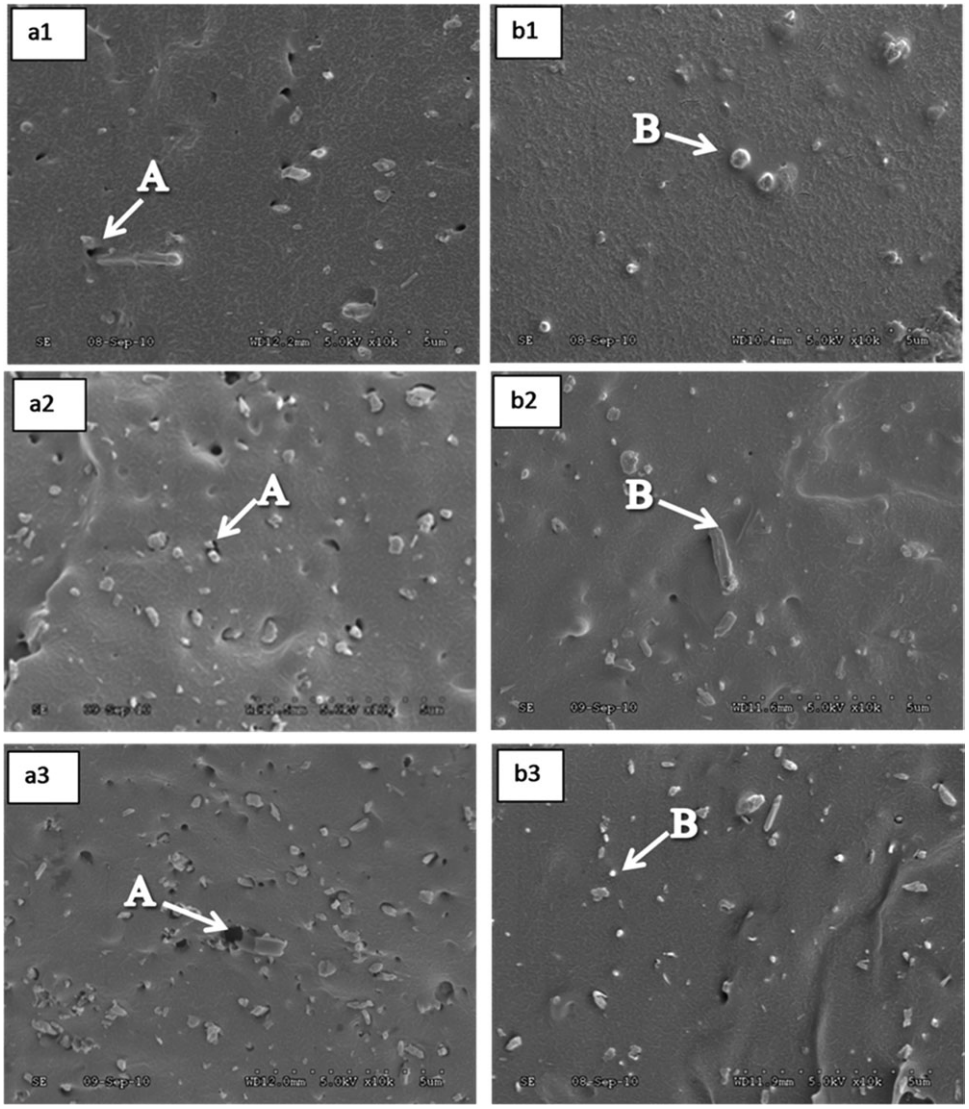

Figure 1. SEM images of PLA/HNT (a, left) and PLA/m-HNT (b, right) nanocomposites filled with (1, up) 2 wt %, (2, middle) 4 wt % or (3, down) 6 wt % HNTs.

Dynamic Mechanical Analysis

Dynamic mechanical properties were measured with a DMA instrument (DMA +150, MetraviB, France) operating in tensile mode at a frequency of 1 Hz. The displacement amplitude and the static force were 10 μm and 1.0 N, respectively. Data were collected from 25 to 150°C at a scanning rate of 3°C min^{-1}. DMA specimens were cut from injection-molded impact samples in the form of rectangular bars of 4($\pm$0.2) mm * 10 ($\pm$0.5) mm * 30 mm nominal dimensions. Three specimens of each composition were tested.

Mechanical Characterization

Mechanical properties of all compounded materials (neat PLA and nanocomposites) were measured from injection-molded specimens. Tensile properties (strength, modulus, elongation at break) of the molded dog bone specimens were measured using a tensile machine (Model 1185, Instron) at a crosshead rate of 10 mm min^{-1} according to ISO 527 standard. Three point bending properties (strength and modulus) were determined at a thickness to span length ratio of 1 : 16 and a crosshead rate of 2 mm min^{-1} as per ISO 178 standard. Notched Charpy impact tests were carried out on a pendulum impact machine (Model 5101, Zwick, Germany) as per ISO 179-1 standard. All the reported values were calculated as averages over five specimens for each composition. All the materials were stored at 25°C and 50% relative humidity for 1 week before testing.

RESULTS AND DISCUSSION

Morphology

The nanotubes dispersion in the polymer matrix is a key factor for fabricating high-performance polymer nanocomposites. A homogeneous dispersion of halloysites and strong interfacial interactions between polymer matrix and nanotubes can effectively improve the mechanical and thermal properties of polymer nanocomposites.[30–33]

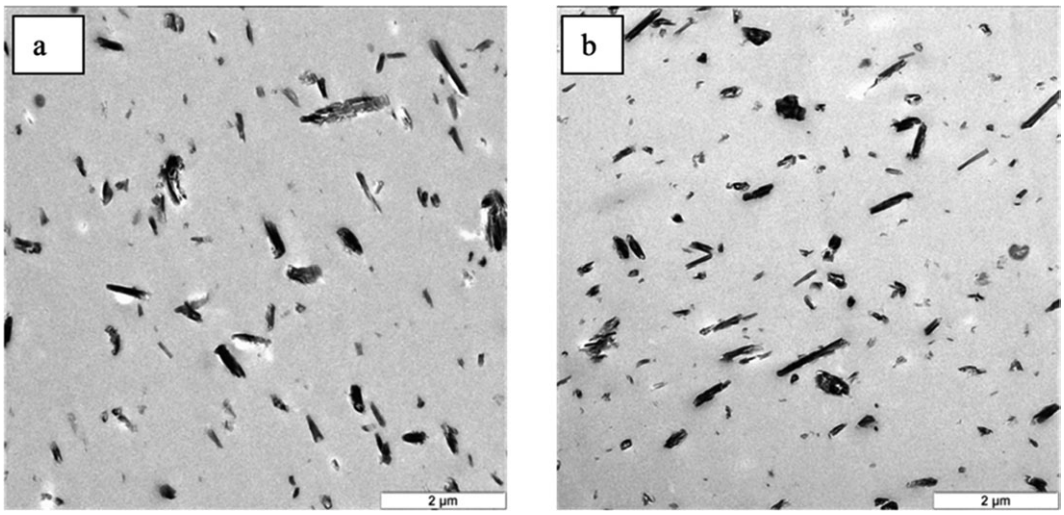

Figure 2. TEM images of 4 wt % PLA/HNT (a, left) and PLA/m-HNT (b, right) nanocomposites.

The SEM images of PLA/HNT and PLA/m-HNT nanocomposites are shown in Figure 1. The dispersion of unmodified halloysites (HNT) is good at 2 and 4 wt % loadings [Figure 1 (a1) and (a2)], whereas numerous aggregates are visible at 6 wt % [Figure 1(a3)]. However, the interface between halloysites and PLA is sharp, and many debonded nanotubes are pulled out from the polymer matrix [marked as "A" in Figure 1(a1–a3)]. This suggests that the interface between HNTs and PLA matrix is weak. In case of PLA/m-HNT nanocomposites, the nanotubes are uniformly dispersed and distributed in the PLA matrix in the entire composition range [Figure 1 (b1–b3)]. Contrary to PLA/HNT nanocomposites, good interface was observed between m-HNTs and PLA matrix. Nearly no debonded nanotubes are observed and nanotubes are visibly embedded in PLA matrix [marked as "*B*" in Figure 1(b1–b3)]. Most m-HNTs are broken rather than pulled out from the PLA matrix. Masterbatch dilution process using high shear extruder is effective in facilitating the dispersion of unmodified halloysites at lower content (2 and 4 wt %) in PLA matrix. Furthermore, modification of halloysites with quaternary ammonium salt improves not only the dispersion at all concentrations (i.e., 2, 4 and 6 wt %) but also the PLA/filler interface compatibility.

Ultrathin slices of 4 wt % halloysites filled PLA/HNT and PLA/m-HNT nanocomposites were further observed by TEM (Figure 2). Dispersion of individual halloysites in PLA/HNT and PLA/m-HNT nanocomposites with minor agglomerates was observed, which is consistent with SEM observations. As a consequence, these observations confirm the efficiency of the melt processing via masterbatch dilution technique to disperse HNTs in PLA matrix.

Thermal Analysis

DSC measurements were carried out to further investigate the influence of HNTs and m-HNTs on the thermal properties of PLA (Figure 3). The shoulder peaks appearing at about 62°C on the DSC heating scan curves of all samples correspond to the glass transition temperature (T_g) of PLA. Addition of HNT or m-HNT nanotubes hardly affects the T_g values of the nanocomposites. Table I summarizes the numerical values obtained from thermograms. Also, neat PLA exhibits during heating an exothermic peak at 122°C due to cold crystallization and a single endothermic peak due to melting. Cold-crystallization of neat PLA occurs in the broad temperature range of 95–125°C. The peak temperature of cold crystallization (T_c) for both PLA/HNT and PLA/m-HNT nanocomposites gradually shifts to lower temperature region with increasing halloysite concentration irrespective of halloysites modification or not. Moreover, the width of the cold crystallization peak decreases with increasing halloysite content. This indicates the nucleation ability of the halloysite, which is in accordance with the literature.[34]

Besides, the shape and the number of the melting peaks depend on halloysites concentration. For neat PLA, a single melting peak is observed. For the formulation containing 2 wt % halloysites, double melting peaks (T_{m1} and T_{m2}) were observed. With increasing halloysites concentration, the peak height located at

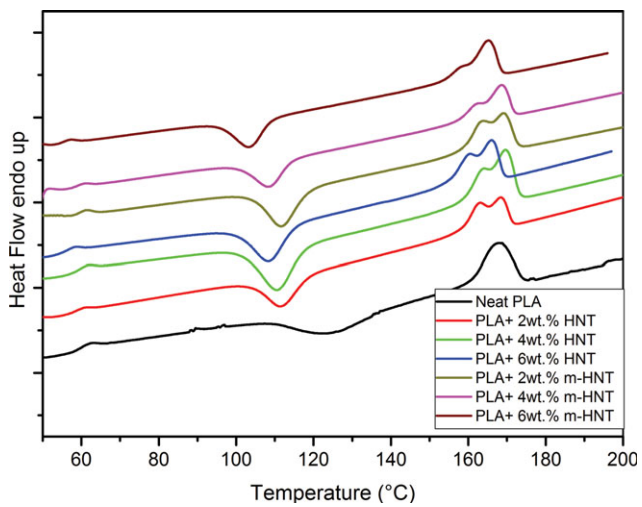

Figure 3. DSC heating scan curves for PLA/HNT and PLA/m-HNT nanocomposites with different HNT concentrations. [Color figure can be viewed in the online issue, which is available at wileyonlinelibrary.com.]

Table I. DSC Heating Scan Values for PLA/HNT and PLA/m-HNT Nanocomposites with Different Halloysite Nanotube Concentrations

Sample	Tensile strength (MPa)	Tensile modulus (MPa)	Elongation at break (%)	Flexural strength (MPa)	Flexural modulus (MPa)	Notched Charpy impact strength (kJ m^{-2})
Neat PLA	54.48 ± 1.62	2923 ± 14	3.6 ± 0.11	82.44 ± 1.21	2877 ± 10	3.38 ± 0.09
PLA/2 wt % HNT	57.98 ± 1.24	3148 ± 18	3.3 ± 0.11	92.23 ± 1.81	3222 ± 12	3.64 ± 0.08
	(+ 6.4%)	(+7.7%)	(−8%)	(+ 11.9%)	(+12.0%)	(+ 7.7%)
PLA/4 wt % HNT	60.67 ± 1.44	3263 ± 16	3.0 ± 0.09	93.15 ± 2.10	3354 ± 10	3.73 ± 0.11
	(+ 11.4%)	(+11.6%)	(−17%)	(+13.0 %)	(+16.6%)	(+ 10.4%)
PLA/6 wt % HNT	62.30 ± 2.21	3378 ± 20	2.6 ± 0.12	93.84 ± 2.24	3615 ± 12	3.71 ± 0.09
	(+ 14.4%)	(+15, 6%)	(−28%)	(+13.8 %)	(+25.7%)	(+ 9.8%)
PLA/2 wt % m-HNT	61.66 ± 1.52	3288 ± 15	3.6 ± 0.08	96.00 ± 1.14	3403 ± 11	3.78 ± 0.10
	(+13.2%)	(+12.5%)	(=)	(+16.4 %)	(+18.3%)	(+ 11.8%)
PLA/4 wt % m-HNT	65.97 ± 1.72	3482 ± 18	3.4 ± 0.11	97.18 ± 2.02	3630 ± 13	3.84 ± 0.10
	(+ 21.1%)	(+19.1%)	(−6%)	(+17.9 %)	(+26.2%)	(+ 13.6%)
PLA/6 wt % m-HNT	70.32 ± 1.92	3644 ± 21	3.2 ± 0.11	97.52 ± 2.12	3764 ± 12	3.88 ± 0.11
	(+ 29.1%)	(+24.7%)	(−11%)	(+18.3 %)	(+30.8%)	(+ 14.8%)

(Δ%): property relative variation compared to neat PLA.

lower temperature decreases while that at higher temperature increases. Such a bimodal melting behavior may be ascribed to a mechanism based on melting of the crystals formed in the cold crystallization stage during heating and followed by recrystallization and further melting processes at higher temperatures, as observed by other authors.[35,36]

Furthermore, the addition of HNT and m-HNT into PLA slightly affects its heat of fusion which increases with growing filler content (Table I). The crystal weight fraction of PLA/HNT increases marginally at lower halloysites contents (2 and 4 wt %) and stabilizes at higher loadings (6 wt %), whereas that of PLA/m-HNT increases significantly with increasing m-HNT

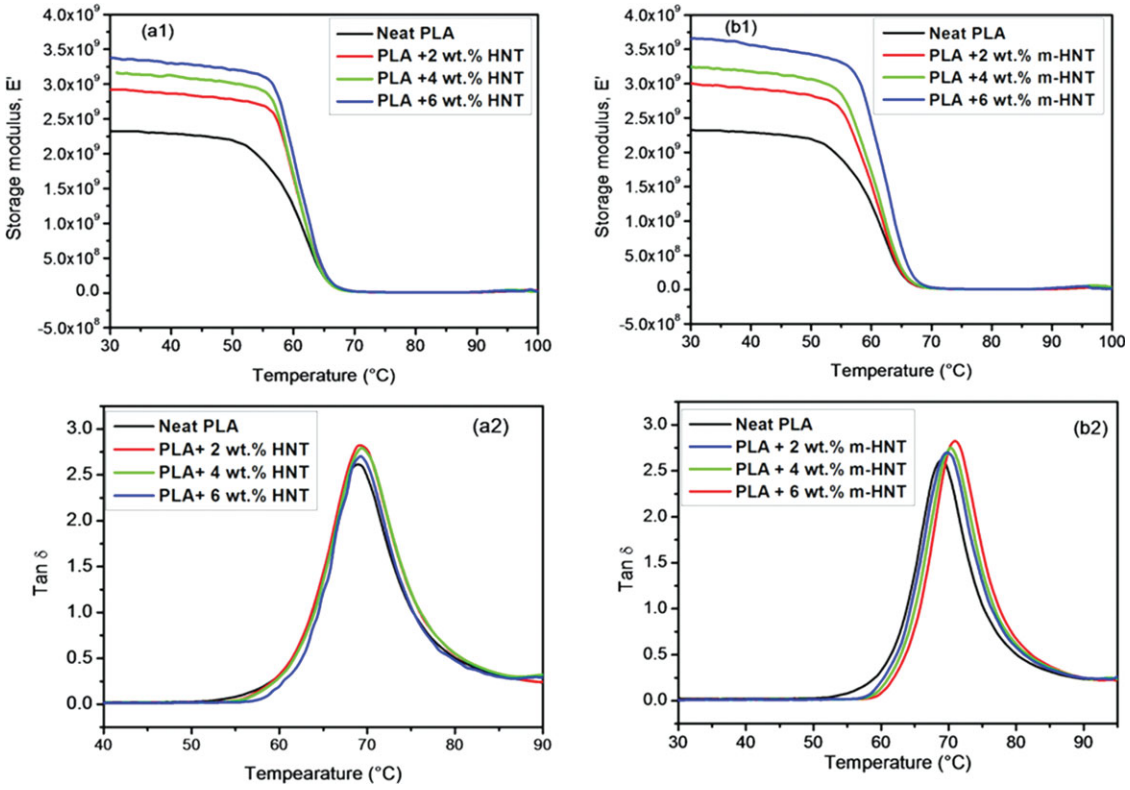

Figure 4. Storage modulus (1, up) and tan δ (2, down) versus temperature at 1 Hz for PLA, PLA/HNT (a, left), and PLA/m-HNT (b, right) nanocomposites. [Color figure can be viewed in the online issue, which is available at wileyonlinelibrary.com.]

Table II. Mechanical Properties of PLA/HNT and PLA/m-HNT Nanocomposites with Different Halloysite Nanotube Concentrations

Sample	T_g (°C)	ΔH_m (J g^{-1})	ΔH_c(J g^{-1})	T_c (°C)	T_{m1} (°C)	T_{m2} (°C)	χ_c (%)
Neat PLA	59	22.62	21.30	120	-	168	10.10
PLA/2 wt % HNT	59	23.72	21.10	114	163	168	11.05
PLA/4 wt % HNT	59	24.77	21.87	111	163	169	12.09
PLA/6 wt % HNT	58	24.98	22.15	109	160	166	12.00
PLA/2 wt % m-HNT	59	24.71	21.33	114	163	169	13.90
PLA/4 wt % m-HNT	60	25.04	21.49	110	162	168	15.14
PLA/6 wt % m-HNT	59	26.42	21.52	107	160	163	19.31

concentration. These results indicate that both nanofiller types act as nucleating agents, the PLA/m-HNT nanocomposites being relatively more crystalline than PLA/HNT nanocomposites. The lower crystallinity exhibited by PLA/HNT nanocomposites may be attributed to the weak interface and the creation of agglomerates at higher loading, leading to reduction of the number of available nucleation sites, thereby minimizing crystallinity.

Dynamic Mechanical Analysis

The storage modulus (E') and the loss factor (tan δ) peaks were recorded as a function of temperature for both PLA/HNT and PLA/m-HNT nanocomposites (Figure 4).

In the glassy region (below 65°C), a general increase of E' is observed with increasing nanofiller content for each series of nanocomposites. Also, the PLA/m-HNT nanocomposites exhibit higher values of E' compared with that of PLA/HNT nanocomposites.

The tan δ peaks of PLA/HNT nanocomposites broaden and slightly shift to higher temperatures compared to that of neat PLA. However, the temperature shift remains constant irrespective of the amount of HNT in the nanocomposites. In case of m-HNT filled nanocomposites, along with broadening of tan δ peaks, increase in peak temperature is observed with increasing m-HNT content. Broadening of tan δ and eventual shift to higher temperatures for nanocomposites indicate a reduction in the segmental motions of the polymer matrix.[37] As a result, it is possible to state that both nanoreinforcements were able to affect the segmental motions of neat PLA. However, magnitude of this effect was higher in PLA/m-HNT compared with PLA/HNT, which may be ascribed to the better interfacial interactions between PLA and m-HNT, causing additional restrictions to the polymer mobility when compared with that of PLA/HNT nanocomposites.

Tensile Properties

Results of tensile testing are summarized in Table II for neat PLA and its nanocomposites. Regarding the PLA/HNT nanocomposites, strength and modulus increase with increasing HNT concentration. The highest modulus is obtained at a 6 wt % HNT content (~15% increase) indicating a modest reinforcement effect of HNT in PLA. The elongation at break slightly decreases with increasing HNT content, but it is retained close to that of the neat matrix at lower HNTs content (i.e. 2 and 4 wt % HNT). In the case of PLA/m-HNT nanocomposites, the tensile strength and the Young's modulus also increase with increasing m-HNT content, the magnitude of increase being much higher (up to ~29 and 25%, respectively) than that observed in the case of PLA filled with 6 wt % unmodified HNT, but without significant embrittlement (very limited decrease of elongation at break). This achievement may be attributed to the good interfacial compatibility between m-HNTs and PLA.

To further explain and confirm the origin of the reinforcing efficiency of halloysites, the tensile properties were further interpreted using micromechanics. The load transfer efficiency within the prepared nanocomposites was assessed by comparing the theoretical modulus computed from the Halpin-Tsai model with experimental data. Halpin-Tsai model was originally developed for fiber-reinforced composite materials. It supposes a random distribution and orientation of the fillers through the polymer matrix, which is generally not the case for injection-molded parts. Nevertheless, it was already successfully used to model the mechanical behavior of injection-molded composites and nanocomposites[38–40] and its applicability in this study can therefore reasonably be assumed. The modified Halpin-Tsai equation for the theoretical modulus of the nanocomposite E_c is given by eq. (2):[41]

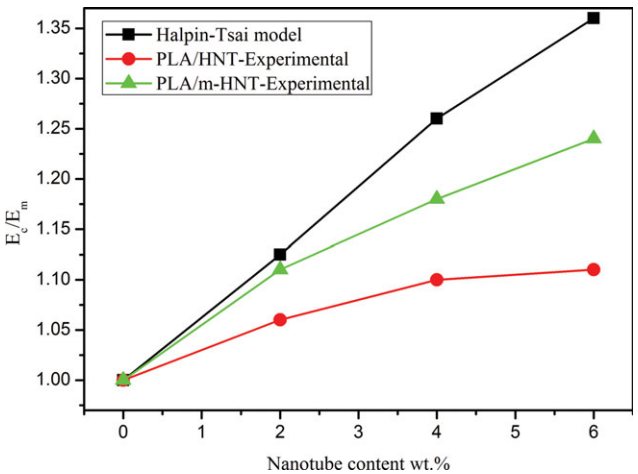

Figure 5. Theoretical and experimental relative Young's modulus versus nanotube concentration for PLA/HNT and PLA/m-HNT nanocomposites. [Color figure can be viewed in the online issue, which is available at wileyonlinelibrary.com.]

$$\frac{E_c}{E_m} = \frac{3}{8}\frac{1 + 2\left(\frac{L_{NT}}{d_{NT}}\right)\eta_L\Phi_f}{1 - \eta_L\Phi_f} + \frac{5}{8}\frac{1 + 2\eta_L\Phi_f}{1 - \eta_T\Phi_f} \quad (2)$$

where

$$\eta_L = \frac{\frac{E_{NT}}{E_m} - 1}{\frac{E_{NT}}{E_m} + 2\left(\frac{L_{NT}}{d_{NT}}\right)} \quad (3)$$

$$\eta_L = \frac{\frac{E_{NT}}{E_m} - 1}{\frac{E_{NT}}{E_m} + 2} \quad (4)$$

where E_c, E_{NT}, and E_m are the Young's modulus of composite, nanotube (300 GPa[42]), and matrix, respectively (2.9 GPa, from Table II); Φ_f the volume fraction of the filler; lNT and dNT the length and diameter of the HNTs (1200 nm and 80 nm respectively). The volume fraction of halloysites in the nanocomposites was calculated from the halloysite weight fraction (2, 4, or 6 wt %), halloysite density (2.5 g cm^{-3}), and PLA density (1.25 g.cm^{-3}). The relative experimental increase of Young's modulus (E_m/E_c) along with the predictions from Halpin-Tsai model for the different types and contents of halloysites is plotted in Figure 5. The experimental values measured for PLA/HNT nanocomposites largely deviated from calculated ones, whereas those obtained for PLA/m-HNT are closer to theoretical predictions. If one assumes that there is no large modification of the filler orientation induced by the shear flow between the two types of samples, this result supports that the externally applied mechanical stress efficiently transfers from the PLA matrix to m-HNTs owing to the good interfacial compatibility between modified nanotubes and the PLA matrix.

Along with tensile modulus, tensile yield stress also needs to be considered to prove the reinforcement efficiency of fillers. The tensile yield stress depends on the constituent properties along with shape and dimension, very importantly, the filler/matrix interphase and the interaction strength. The yield stress can be theoretically predicted using the Pukanszky model,[43,44] which assumes that an interphase forms spontaneously in composites and that the yield stress changes proportionally to its actual value as a function of filler volume fraction according to eq. (5):

$$\sigma_y = \sigma_{ym}\frac{1 - \Phi_f}{1 + 2.5\,\Phi_f}e^{B\,\Phi_f} \quad (5)$$

where σ_y and σ_{ym} are the yield stress of the composite and the matrix, respectively, Φ_f the volume fraction of the filler in the composites, and B a parameter characterizing the degree of filler/matrix interaction. The term $(1-\Phi_f)/(1 + 2.5\ \Phi_f)$ expresses the effective load-bearing cross-sectional area of the matrix. From this equation, the reduced yield stress σ_{red} can be defined as:

$$\mathrm{Ln}[\sigma_{red}] = \mathrm{Ln}\left(\frac{1 + 2.5\,\Phi_f}{1 - \Phi_f}\sigma_y\right) = \mathrm{Ln}[\sigma_{ym}] + B\,\Phi_f \quad (6)$$

When plotting $\mathrm{Ln}[\sigma_{red}]$ as a function of the filler volume fraction Φ_f, the "B" interaction parameter is obtained from the slope of the straight line. However, using eq. (6) requires to know the exact value of the yield stress of the structurally unaffected matrix σ_{ym}, which can be different from that of neat PLA because of the structural modifications locally induced by the addition of the fillers. To avoid this difficulty, it is possible to calculate a relative yield stress σ_{rel}, which does not require the value of the matrix yield stress, according to eq. (7):

$$\sigma_{rel} = \frac{\sigma_y}{\sigma_{ym}}\frac{1 + 2.5\,\Phi_f}{1 - \Phi_f} \quad (7)$$

which can be arranged in a linear form as follows:

$$\mathrm{Ln}[\sigma_{red}] = \mathrm{Ln}\left(\frac{\sigma_y}{\sigma_{ym}}\frac{1 + 2.5\,\Phi_f}{1 - \Phi_f}\right) = B\,\Phi_f \quad (8)$$

Now, when plotting $\mathrm{Ln}[\sigma_{rel}]$ as a function of filler volume fraction, Φ_f the "B" interaction parameter is easily determined from the linear curve. Generally, if the value of B is zero, the filler acts as a void, and the value of "B" depends on the factor influencing the load bearing capacity such as strength and thickness of the interface. Therefore, higher the "B" value, better the interfacial compatibility (via thickness and/or strength). As per the reported literature, the "B" value for polymer nanocomposites ranges between 2 and 15 depending on the interaction level.[40] In this study, Pukanszky model was applied to evaluate the interfacial interactions in PLA/HNT and PLA/m-HNT nanocomposites. The plot of $\mathrm{Ln}[\sigma_{rel}]$ as a function of filler volume fraction Φ_f is shown in Figure 6. The interaction parameter B was deduced from the linear fit of the experimental data points. The parameter B corresponding to PLA/m-HNT (e.g., 8.6) is higher and almost double than that of the PLA/HNT nanocomposites (e.g., 4.5). Higher value of B interaction coefficient for PLA/m-HNT nanocomposites is due to a better interface between modified halloysites and PLA compared with unmodified halloysites in PLA. This is clearly evidenced by the relatively better mechanical and thermal properties of PLA/m-HNT

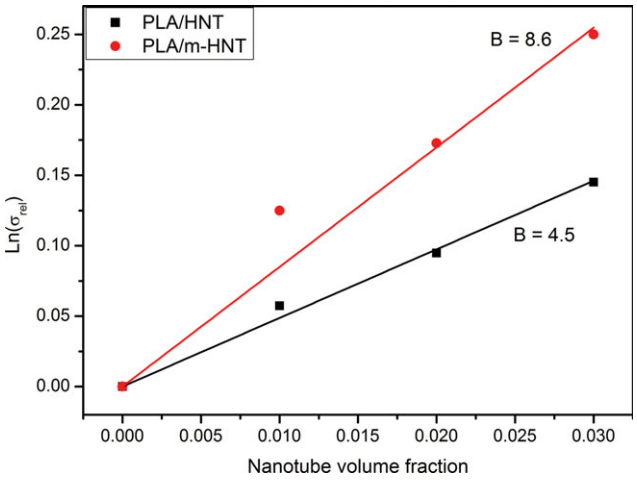

Figure 6. Evaluation of "B" interaction parameter for PLA/HNT and PLA/m-HNT nanocomposites using Pukanszky model. [Color figure can be viewed in the online issue, which is available at wileyonlinelibrary.com.]

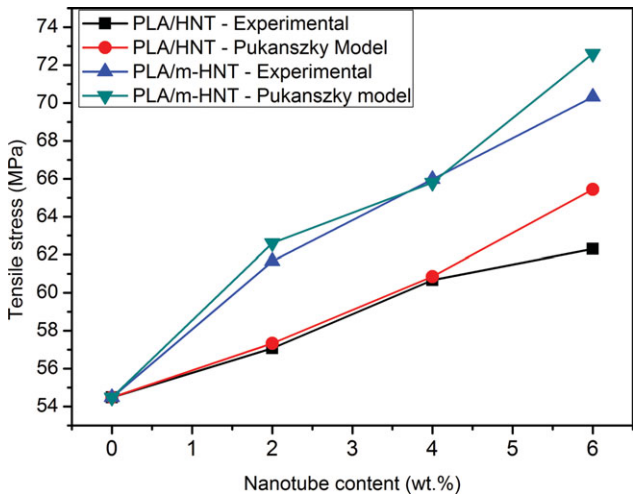

Figure 7. Theoretical and experimental tensile yield stress versus nanotube concentration for PLA/HNT and PLA/m-HNT nanocomposites. [Color figure can be viewed in the online issue, which is available at wileyonlinelibrary.com.]

nanocomposites compared with PLA/HNT nanocomposites. Finally, the validity of the model with the obtained *B* value (interaction parameter) was checked by comparing the measured tensile yield stress values with those calculated using Pukanszky model (Figure 7). Experimental values match Pukansky predictions quite well, therefore confirming that Pukanszky model is valid for the studied system.

Bending and Impact Properties

Flexural properties of neat PLA and its nanocomposites are reported in Table II. A significant increase in the flexural strength and modulus is observed for PLA/m-HNT nanocomposites (+18.3 % and + 30.8 % at 6 wt %, respectively). There is not so much increase for PLA/HNT nanocomposites (only + 13.8 % and + 25.7 % at 6 wt %, respectively), which is attributed to the debonding of the nanofillers from the matrix.

The effect of nanotubes content on the Charpy impact strength of notched samples of both PLA/HNT and PLA/m-HNT nanocomposites is also reported in Table II. In both cases, the impact strength increases gradually with nanotubes addition and saturates at 6 wt % halloysites, reaching +10 and +15% at that content for PLA/HNT and PLA/m-HNT nanocomposites, respectively. The moderate reinforcement effect in PLA/HNT nanocomposites is due to good dispersion of individual nanotubes in PLA at concentrations as high as 6 wt %, as shown previously by microscopy. The slightly higher reinforcing effect observed in PLA/m-HNT nanocomposites is due not only to the halloysites good dispersion but also to the good interfacial compatibility between PLA and nanotubes, as indicated by Pukanszky model.

CONCLUSIONS

Novel PLA/halloysites nanocomposites based on both unmodified halloysites (HNT) and quaternary ammonium salt with benzalkonium chloride treated halloysites (m-HNT) were successfully prepared by melt compounding in a high shear twin-screw extruder via masterbatch dilution process. A homogeneous dispersion of the nanotubes was obtained in the PLA matrix. The degree of crystallinity of PLA/m-HNT nanocomposites is slightly higher than that of PLA/HNT owing to the contribution of m-HNT as an effective nucleating agent. Compared to neat PLA, significant enhancements in stiffness and yield stress are obtained with only low loadings of filler, the elongation at break being almost constant. The increase of PLA usage properties (i.e., tensile and bending moduli and/or strengths and impact strength) on halloysites addition is higher for m-HNT than for HNT. Using micromechanical modeling based on Halpin-Tsai and Pukanszky models, it was possible to ascribe this superior reinforcement efficiency of m-HNT to the better interfacial compatibility induced by the modification of the nanotube surface.

ACKNOWLEDGMENTS

The authors are indebted to CISIT (International Campus on Safety and Intermodality in Transportation), the Nord-Pas-de-Calais Region and the European Community (FEDER, European Funds for Regional Development) for funding of the twin-screw extruder and the DMA equipment. Thanks are also due to the master student Moussa KHALFALLAH for his contribution to materials processing and characterization.

REFERENCES

1. Lim, L. T.; Auras, R.; Rubino, M. *Prog. Polym. Sci.* **2008,** *33*, 820.
2. Lunt, J. *Polym. Degrad. Stab.* **2008,** *59*, 145.
3. Anders, S.; Mikael, S. *Prog. Polym. Sci.* **2002,** *27*, 1123.
4. Kontou, E.; Niaounakis, M.; Georgiopoulos, P. *J. Appl. Polym. Sci.* **2011,** *133*, 1519.
5. Fukushima, K.; Murariu, M.; Camino, G.; Dubois, P. *Polym. Degrad. Stab.* **2010,** *95*, 1063.
6. Papageorgiou, G. Z.; Achilias, D. S.; Nanaki, S.; Beslikas, T.; Bikiaris, D. *Thermochim. Acta* **2010,** *511*, 129.
7. Matusik, J.; Stodolak, E.; Bahranowski, K. *Appl. Clay Sci.* **2011,** *51*, 102.
8. Wu, C. S.; Liao, H. T. *Polymer* **2007,** *48*, 4449.
9. Wu, D.; Wu, L.; Zhang, M.; Zhao, Y. *Polym. Degrad. Stab.* **2008,** *93*, 1577.
10. Prashantha, K.; Soulestin, J.; Lacrampe, M. F.; Krawczak, P. *Polym. Polym. Comp.* **2009,** *17*, 205.
11. Paul, M. A.; Delcourt, C.; Alexandre, M.; Degee, P.; Monteverde, F.; Rulmont, A.; Dubois, P. *Macromol. Chem. Phys.* **2005,** *206*, 484.
12. Hedicke-Höchstötter, H.; Lim, G. T.; Altstädt, V. *Compos. Sci. Technol.* **2009,** *69*, 330.
13. Liu, M.; Guo, B.; Du, M.; Chen, F.; Jia, D. *Polymer* **2009,** *50*, 3022.
14. Lecouvet, B.; Sclavons, M.; Bourbigot, S.; Devaux, J.; Bailly, C. *Polymer* **2011,** *52*, 4284.
15. Prashantha, K.; Lacrampe, M. F.; Krawczak, P. *Express Polym. Lett.* **2011,** *5*, 295.

16. Prashantha, K.; Schmitt, H.; Lacrampe, M. F.; Krawczak, P. *Compos. Sci. Technol.* **2011,** *71*, 1859.
17. Schmitt, H.; Prashantha, K.; Soulestin, J.; Lacrampe, M. F.; Krawczak, P. *Carbohydr. Polym.* **2012,** *89*, 920.
18. Du, M.; Guo, B.; Jia, J. *Polym. Int.* **2010,** *59*, 574.
19. Singh, B. *Clay Miner.* **1996,** *44*, 191.
20. Frost, R. L.; Shurvell, H. F. *Clay Miner.* **1997,** *45*, 68.
21. Qi, R.; Guo, R.; Shen, M.; Cao, X.; Zhang, L.; Xu, J.; Yu, J.; Shi, X. *J. Mater. Chem.* **2010,** *20*, 10622.
22. Qi, R.; Cao, X.; Shen, M.; Guo, R.; Yu, J.; Shi, X. *J. Biomater. Sci. Polym. Ed.* **2012,** *23*, 299.
23. Vergaro, V.; Abdullayev, E.; Lvov, Y. M.; Zeitoun, A.; Cingolani, R.; Rinaldi, R.; Leporatti, S. *Biomacromolecules* **2010,** *11*, 820.
24. Price, R. R.; Gaber, B. P.; Lvov, Y. *J. Microencapsul.* **2001,** *18*, 713.
25. Shchukin, D.; Price, R.; Sukhorukov, G.; Lvov, Y. *Small (Nano, Micro)* **2005,** *1*, 510.
26. Kelly, H.; Deasy, P.; Ziaka, E.; Claffey, E. N. *Int. J. Pharm.* **2004,** *274*, 167.
27. Zhou, W.; Guo, B.; Liu, M.; Liao, R.; Rabie, A.; Jia, D. *J. Biomed. Mater. Res. Part A* **2010,** *93*, 1574.
28. Bertagnolli, C.; De Araujo, A. L. P.; Kleiniibing, S.; Da Silva, M. G. C. *Chem. Eng. Trans.* **2011,** *24*, 1537.
29. Gamez-Perez, J.; Nascimento, L.; Bou, J. J.; Franco-Urquiza, E.; Santana, O. O.; Carrasco, F.; Maspoch, M. L. *J. Appl. Polym. Sci.* **2011,** *120*, 896.
30. Hong, C. E.; Lee. J. H.; Prashantha, K.; Advani, S. G. *Compos. Sci. Technol.* **2007,** *67*, 1027.
31. Prashantha, K.; Soulestin, J.; Lacrampe, M. F.; Krawczak, P.; Dupin, G.; Claes, M. *Compos. Sci. Technol.* **2009,** *69*, 1756.
32. Gupta B.; Lacrampe, M. F.; Krawczak, P. *Polym. Polym. Comp.* **2006,** *14*, 13.
33. Prashantha, K.; Soulestin, J.; Lacrampe, M. F.; Claes, M.; Dupin, G.; Krawczak, P. *Express Polym. Lett.* **2008,** *2*, 735.
34. Yoon, J. T.; Jeong, Y. G.; Lee, S. C.; Min, B. G. *Polym. Adv. Technol.* **2009,** *20*, 631.
35. Wu, D.; Wu, L.; Wu, L.; Xu, B.; Zhang, Y.; Zhang, M.; *J. Polym. Sci. Part B: Polym. Phys.* **2007,** *45*, 1100.
36. Huang, J. W.; Hung, Y. C.; Wen, Y. L.; Kang, C. C.; Yeh, M. Y. *J. Appl. Polym. Sci.* **2009,** *112*, 3149.
37. Alexandre, M.; Dubois, P. *Mater. Sci. Eng. R: Rep.* **2000,** *28*, 1.
38. Chen, G. X.; Kim, H. S.; Park, B. H.; Yoon, J. S. *Polymer* **2006,** *47*, 4760.
39. Gansz, M.; Satapathy, B. K.; Thunga, M.; Weidisch, R.; Pötschke, P.; Jehnichen, D. *Acta Mater.* **2008,** *56*, 2247.
40. Dayma, N.; Satapathy, B. K. *Mater. Des.* **2010,** *31*, 4693.
41. Zhang, X.; Liu, T.; Sreekumar, T. V.; Kumar, S.; Moore, V. C.; Hauge, R. H.; Smalley, R. E. *Nano Lett.* **2003,** *9*, 1285.
42. Guimaraes, L.; Enyashin, A. N.; Seifert, G.; Duarte, H. A. *J. Phys. Chem. C* **2010,** *114*, 11358.
43. Renner, K.; Móczó, J.; Vörös, G.; Pukánszky, B. *Eur. Polym. J.* **2010,** *46*, 2000.
44. Százdi, L.; Pukánszky, Jr.; B.; Vancso, G. *J. Polymer* **2003,** *47*, 4638.